Laboratory Generation of Free Chlorine from HCl Under Stratospheric Afterburning Conditions

1 March 1996

Prepared by

M. L. BURKE and P. F. ZITTEL
Space and Environment Technology Center
Technology Operations
Engineering and Technology Group

Prepared for

SPACE AND MISSILE SYSTEMS CENTER
AIR FORCE MATERIEL COMMAND
2430 E. El Segundo Boulevard
Los Angeles Air Force Base, CA 90245

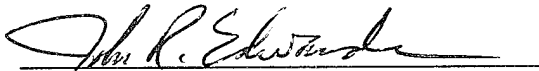Space Technology Applications

19960522 059

THE AEROSPACE
CORPORATION
El Segundo, California

John R. Edwards
SMC/CEV

REPORT DOCUMENTATION PAGE

1. AGENCY USE ONLY (*Leave blank*)	2. REPORT DATE 1 March 1996	3. REPORT TYPE AND DATES COVERED

4. TITLE AND SUBTITLE

Laboratory Generation of Free Chlorine from HCl Under Stratospheric Afterburning Conditions

5. FUNDING NUMBERS

F04701-93-C-0094

6. AUTHOR(S)

Burke, Martin L., and Zittel, Paul F.

7. PERFORMING ORGANIZATION NAME(S) AND ADDRESS(ES)

The Aerospace Corporation
Technology Operations
El Segundo, CA 90245-4691

8. PERFORMING ORGANIZATION REPORT NUMBER

TR-96(1306)-3

9. SPONSORING/MONITORING AGENCY NAME(S) AND ADDRESS(ES)

Space and Missile Systems Center
Air Force Materiel Command
2430 E. El Segundo Blvd.
Los Angeles Air Force Base, CA 90245

10. SPONSORING/MONITORING AGENCY REPORT NUMBER

SMC-TR-96-10

11. SUPPLEMENTARY NOTES

12a. DISTRIBUTION/AVAILABILITY STATEMENT

Approved for public release; distribution unlimited

12b. DISTRIBUTION CODE

13. ABSTRACT (*Maximum 200 words*)

Experiments have been conducted using a low pressure laboratory flame apparatus to examine the chemistry of solid rocket motor (SRM) afterburning relevant for stratospheric altitudes. It has been found that a significant fraction of the HCl injected into H_2-O_2 and H_2-CO-O_2 flames can be consumed, with observed losses of up to 40%. The extent of conversion of HCl was found to increase with increasing oxygen:fuel (O/F) ratio and decreasing pressure. The loss at a given O/F was also higher for flames with equal flows of H_2 and CO, compared to flames with no CO in the fuel. The major product of HCl reaction was found to be Cl_2, with no other chlorine-containing products observed via mass spectrometry. Distinct Cl_2 $B \rightarrow X$ emission bands were observed, along with very weak ClO $A \rightarrow X$ bands and a bright, white continuum emission, which apparently arises from one or more chlorine-containing compounds. The general findings concerning the magnitude of HCl conversion and the formation of Cl_2 are consistent with published modeling results for SRM stratospheric afterburning. This formation of "free" chlorine could lead to catalytic destruction of ozone in regions near the path the launch vehicle follows during boost through the stratosphere.

14. SUBJECT TERMS

Afterburning
Environmental Impact
Ozone Depletion

15. NUMBER OF PAGES

33

16. PRICE CODE

17. SECURITY CLASSIFICATION OF REPORT Unclassified	18. SECURITY CLASSIFICATION OF THIS PAGE Unclassified	19. SECURITY CLASSIFICATION OF ABSTRACT Unclassified	20. LIMITATION OF ABSTRACT

Preface

Contents

Figures

Table

1. Introduction

In recent years, the potential impacts on stratospheric ozone due to the launch of vehicles with solid-fuel rocket motors (SRMs) have been investigated in a number of computer-modeling studies [1-8]. The main concern is that chlorine-containing compounds released by the SRMs may lead to catalytic destruction of ozone in a region surrounding the exhaust plume. This could then result in enhanced UV radiation at the ground during the first few hours after launch. Model studies of plume expansion and chemical reaction have indicated that extended zones of ozone depletion may occur in the wake of a launch [1,4-7], but this is highly dependent on the identity and quantity of chlorine compounds left in the wake of the launch vehicle. For instance, gaseous HCl is inert toward ozone and is slow to photodissociate in the stratosphere, whereas Cl_2 (which rapidly photodissociates), Cl atoms, or ClO may readily contribute to ozone destruction cycles [1-4,7].

The major exhaust gases, and their mole fractions, at the nozzle exit plane of a Titan IV SRM are H_2 (0.34), CO (0.27), HCl (0.15), H_2O (0.12), and N_2 (0.08) [1]. Mole fractions for the exhaust of Space Shuttle SRMs are similar. There is also a large mass of alumina particles in SRM exhaust, which is not included here in the evaluation of the gas mole fractions. Both the H_2 and CO in the hot exhaust afterburn vigorously upon mixing with ambient air, essentially creating an H_2-CO-O_2 flame. For both Titan IV and the Space Shuttle, this afterburning occurs at all vehicle altitudes during boost through the ozone-rich regions of the stratosphere. There have not yet been field measurements of the products of afterburning for SRMs, at least at stratospheric altitudes. However, computer simulations of afterburning have been performed. These simulations indicate that Cl atoms and Cl_2 should be formed in high abundance from the HCl in the exhaust, with the yield of this "free" chlorine increasing with altitude through the stratosphere [1,3]. Conversions of HCl to free chlorine of approximately 80% have been predicted both for a Titan IV SRM at 40 km [1] and for a smaller SRM at 30 km [3]. Evaluation of the potential for creation of local ozone-depleted regions following a launch is thus dependent on the accuracy of the product composition predicted by these afterburning models.

Experimental tests of these afterburning models would thus be useful in order to evaluate the accuracy of their predictions. A few previous studies exist that are relevant in terms of the flame composition of interest here. The effects of HCl on H_2-O_2 flames has been investigated in terms of potential flame-inhibition effects [9-11], as have other halogen-containing molecules. However, the consumption of HCl and production of other chlorine-containing molecules were not monitored in those studies. Perhaps the most relevant experimental studies in the literature are those of Roesler, Yetter, and Dryer, where the inhibition by HCl of the moist oxidation of CO was examined [12-14]. In that work, HCl was added to an atmospheric pressure reaction system of CO, O_2, and H_2O at temperatures near 1000 K. The flame composition was monitored as a function of reaction time, and HCl losses on the order of 20%–40% were measured. These results support the plausibility of HCl conversion via afterburning. However, the fuel composition, pressure, and temperature of the experiments of Roesler, Yetter, and Dryer are significantly different from the conditions of SRM afterburning.

In order to more accurately test the predictions of computer simulations of afterburning, laboratory experiments have been performed here, whereby conditions relevant to SRM afterburning in the stratosphere have been simulated in a low pressure flame apparatus. The extent of consumption of HCl in the flame under varying conditions has been determined using mass spectrometry, and the formation of other chlorine-containing products has been explored and quantified. In addition, optical emission spectra have been collected from the near-UV to the near-IR in order to identify excited state species in the flame. The results of these experiments are discussed in terms of their bearing on the validity of results of afterburning simulations, and thus on the potential for ozone depletion following a launch.

1

2. Experimental

A low pressure flame apparatus was used to simulate the pressures, temperatures, and compositions that are relevant to stratospheric afterburning of SRM exhaust. The apparatus (Figure 1) consisted of a 3-in.-diam bronze porous disk burner mounted inside a 6-in.-i.d. stainless steel flow tube, which was pumped by a 50 cfm Welch 1398 vacuum pump. Flame ignition was achieved with a brief electrical discharge from a Tesla coil. Immediately downstream of the burner were windows that allowed the flame to be viewed and flame emission spectra to be acquired.

The burner was water cooled and consists of a 2-in.-diam inner core and an outer ring. N_2 was flowed through the outer ring to contain the flame, to keep the walls near the flame region relatively cool, and to dilute unburned reactants before they reached the pump. However, all other gases used were premixed and injected through the inner core of the burner. In previous work with N_2-contained H_2-O_2 flames in this apparatus, flame temperatures as high as approximately 2650 K were measured [15]. For a given flow rate, the flame pressure was controlled using a valve between the flame tube and the pump, and a liquid-nitrogen-cooled trap located before the pump removed water and other condensable products, such as chlorine-containing species.

A mass spectrometer sampling system was integrated into the flame apparatus to allow the products of combustion to be monitored. A quartz sampling probe was mounted 3 ft downstream of the burner, with the tip of the probe protruding into the center of the flame tube (Figure 1). Flame effluent gases were expanded across an orifice at the end of the quartz probe and were rapidly pumped through a Teflon sampling line. The sampling line branched to a variable leak valve that was used to control the flow into the mass spectrometer chamber. An Extrel quadrupole mass spectrometer was used in the positive ion detection mode, using 70 eV electrons for ionization. The mass spectrometer chamber was pumped with a 450 l/s turbo pump and had a base pressure of 1×10^{-7} torr. Under typical conditions, the flame was operated at 40 torr, the sampling line pressure was 2.5 torr, and the mass spectrometer chamber pressure was 2×10^{-7} torr.

In order to discriminate against background gases in the mass spectrometer chamber, the flow of gases from the flame effluent sampling line was modulated prior to entering the mass spectrometer ionizer. Flame gases introduced into the mass spectrometer chamber were flowed through an approximately 0.4-in.-long, 0.02-in.-i.d. needle, with an 800 Hz tuning fork chopper located at the needle exit. This chopped beam assembly was mounted as close to the mass spectrometer ionizer as possible, and was optically aligned with the ionizer orifice. The mass spectrometer signals for gases introduced through the sampling line were found to be modulated by approximately 40% using this configuration. A lock-in amplifier was used to process the resulting signals.

A variety of flame conditions were explored in order to characterize the effects of pressure and composition on flame products. The pressure inside the flame tube was varied from 16 to 40 torr, corresponding to an altitude range of 20 to 26 km. This range brackets the region of the stratosphere where ozone concentrations are highest. Two different fuel mixtures were used in these experiments, with the first consisting of H_2 and HCl in a 4:1 molar ratio, and the second consisting of H_2, CO, and HCl in a 2:2:1 mix. For both cases, a flow of Ar equal to the HCl flow was mixed in with the fuel, and the flow of N_2 through the outer burner ring was 30 times the HCl flow. The flow of O_2 was varied from 1.6 to 4 relative to HCl, which corresponds to a range of oxygen:fuel (O/F) ratios of 0.8 to 2 for each of the fuel compositions used. Here, O/F is defined as the flow of O_2 into the flame relative to the O_2 flow

Sampling Line (2.5 torr)

Burner

P=10^{-7} torr

Quadrupole Mass
Spectrometer

N_2
(outer ring)

Other
Gases
(core)

P = 16 - 40 torr   To Pump

To
Pump

Quartz Window

Array
Detector

Grating
Spectrometer

Typical Flows (slm)
HCl-Seeded H_2-O_2 Flame,
O/F = 1, P = 40 torr

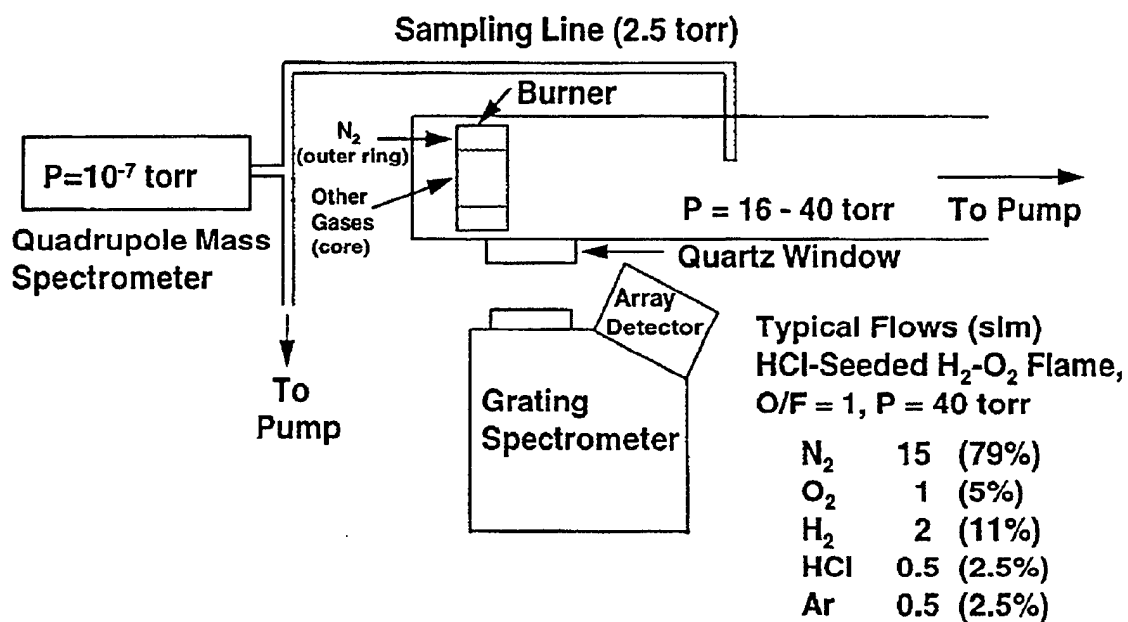|		
N_2	15	(79%)
O_2	1	(5%)
H_2	2	(11%)
HCl	0.5	(2.5%)
Ar	0.5	(2.5%)

Figure 1.   Schematic of Laboratory Flame Apparatus. Typical flow rates are
listed in standard liters per minute for a stoichiometric HCl-seeded H_2-
O_2 flame at 40 torr.

required to fully oxidize the H_2 and CO in the fuel to H_2O and CO_2, respectively. For a stoichiometric mixture, O/F is thus equal to 1. The HCl content of the fuel was not included in the determination of O/F. The flows of all gases injected into the flame were monitored using Edwards calibrated mass flow meters.

The relative flow of N_2 was kept high due to atmospheric abundance, and also to provide a diluent gas to reduce explosion hazards in the flame tube, pump, and pump exhaust line in the event that high flows of unburned H_2 may survive past the flame region. Ar was used as an inert calibration gas for the mass spectrometer, and the injection of the Ar into the fuel stream prior to flow through the burner ensured that there would not be anomalous results due to incomplete mixing in the flame tube. Since most of the chemical species of interest–e.g., HCl, Cl_2–have relatively high molecular weights, Ar was an ideal calibrant in terms of matching gas diffusion rates. Mass spectral sensitivities of all reactant gases were calibrated relative to Ar with the flame off, allowing the composition of the flame effluent to be quantitatively determined. Sensitivities for the product molecules CO_2 and Cl_2 were also calibrated.

Experiments conducted over a broad range of flame conditions were performed with the primary intent of quantifying the fraction of HCl converted to products in the flame. For these experiments, mass spectral data were acquired over the range of 1 to 50 a.m.u. only, since all of the reactants and most of the flame products could be monitored in this region. The high signal-to-noise ratio for molecules such as HCl, H_2, O_2, CO, CO_2, and H_2O allowed data to be acquired rapidly, and thus a broad range of flame conditions was efficiently examined. The identification of chlorine-containing flame products, however, required covering a broad mass range under high sensitivity. Thus, lengthy signal averaging was required. For this reason, product surveys were only conducted for conditions where high yields of chlorine-containing products (other than HCl) were expected, i.e., where high fractional losses of HCl were observed. The mass range covered in these product searches extended to 100 a.m.u.

In addition to mass spectrometer sampling, the flame was examined via optical emission spectroscopy. A McPherson 0.3 m grating spectrograph coupled with an EG&G OMA 3 array detector was used to collect emission spectra over the range from 275 to 900 nm. A 500 nm blazed grating was used for all measurements, and long-wavelength pass filters with 50% transmittance points at 295 and 475 nm were used over the 325-500 nm and 500-900 nm spectral regions, respectively, to ensure that only first-order diffraction features were recorded. Entrance slit widths of 50 to 200 μm were used. The relative wavelength-dependent sensitivity of the spectrograph/OMA was determined using a calibrated quartz-halogen tungsten filament lamp. This sensitivity was used, along with measured filter transmittances, to convert experimental emission intensities to relative photon yields. The quartz window through which emissions were measured had a nominal internal transmittance of greater than 97% over the full wavelength range examined. Thus, any wavelength-dependent transmission variations were neglected for the determination of relative emission intensities. No coupling lenses were employed during the collection of emission spectra, and based on the f5.3 spectrograph optics, the portion of the flame that was viewed was calculated to cover the range from approximately 0.5–2.5 in. downstream of the burner.

5

3. Results

3.1. Mass Spectrometry

We have found that a significant fraction of the HCl injected into H_2-O_2 and H_2-CO-O_2 flames can be consumed, particularly at high O/F ratios. For a flame pressure of 40 torr, which corresponds to an altitude of 20 km, as the O/F ratio for an HCl-seeded H_2-O_2 flame is varied from 0.8 to 2.0, the fractional loss of HCl increases from 0.0 to 0.28 (Figure 2). For the H_2-CO-O_2 flame, the rise in HCl loss with O/F is sharper, and at an O/F of 2.0, the fractional loss of HCl is 0.33. For both of these data sets, the minimum fractional loss is approximately -0.025, indicating that the relative mass spectrometer sensitivity for HCl with the flame on is slightly different than that measured during calibration with the flame off. The actual HCl loss values thus may be slightly higher than the values plotted and mentioned here, but this error in the HCl fractional loss is no greater than the offset of 0.025 observed at low O/F values. The HCl fractional losses measured at O/F = 2.0 for different flame conditions are listed in Table 1.

The curves drawn through the data points in Figure 2 are simple illustrative fits using the functional form $Y = Y_0 + (Y_{max}-Y_0)\{1 - exp[C(X_0 - X)]\}^2$ for $X \geq X_0$, and $Y = Y_0$ for $X < X_0$. Here, X and Y denote the O/F ratio and HCl fractional loss, respectively; the parameter Y_0 represents the minimum HCl loss; Y_{max} is an asymptotic maximum loss; C determines the steepness of the rise of the HCl loss with increasing O/F; and X_0 is a threshold O/F value, below which the HCl loss is equal to the minimum value. This functional form was chosen because it reproduces the general behavior of the data with a minimal number of adjustable parameters. The fitting of the function to data was performed using a least-squares gradient method.

When the flame pressure was reduced from 40 to 16 torr by proportionally lowering all of the gas flow rates, the recorded fractional losses of HCl at O/F of 2.0 were somewhat higher (Figure 3). For the H_2-O_2 and H_2-CO-O_2 flames, the measured HCl fractional losses at O/F = 2.0 were 0.32 and 0.40, respectively. Again, the minimum measured losses were negative (approximately -0.035). Thus, the actual losses at O/F of 2 may be slightly higher than the stated values. The 16 torr pressure for these experiments corresponds to an altitude of 26 km.

In addition to the magnitude of the HCl losses measured at O/F = 2, there are other notable differences between the results for flame pressures of 40 and 16 torr. For 40 torr flames, the HCl loss rises fairly sharply with O/F and appears to closely approach an asymptotic value by O/F of 2, particularly for the H_2-CO-O_2 flame. However, for the 16 torr flame, the rise in HCl loss with O/F is more gradual, and the HCl loss at O/F of 2 appears to be somewhat shy of an asymptotic value. It is thus likely that somewhat higher fractional losses of HCl may be achieved for O/F values greater than 2. For both pressures, however, the HCl conversion at a given O/F is considerably higher for the H_2-CO-O_2 flame than for the H_2-O_2 flame.

Cl_2 was found to be a major product of HCl conversion, but no other chlorine-containing products, such as ClO, ClO_2, or Cl_2O, were observed via mass spectrometry. The search for chlorine-containing products, other than HCl, was limited to the highest O/F examined of 2.0, since the highest observed fractional losses of HCl were for this O/F. The mass range from 45 to 100 a.m.u. was carefully examined for HCl-seeded flames at 40 torr and 16 torr for both H_2-O_2 and H_2-CO-O_2 flames, and the mass spectral signature of Cl_2 was clearly identified for all of these conditions. The 70, 72, and 74 a.m.u. signals

7

Figure 2.   HCl Conversion in Flames at 40 torr. The fraction of HCl consumed is
shown as a function of the O/F ratio for an H_2-O_2 flame with an
H_2:HCl ratio of 4:1 (filled squares), and for an H_2-CO-O_2 flame with
an H_2:CO:HCl ratio of 2:2:1 (open squares).

8

Table 1. Comparison of Experimental and Model Values for HCl Consumption

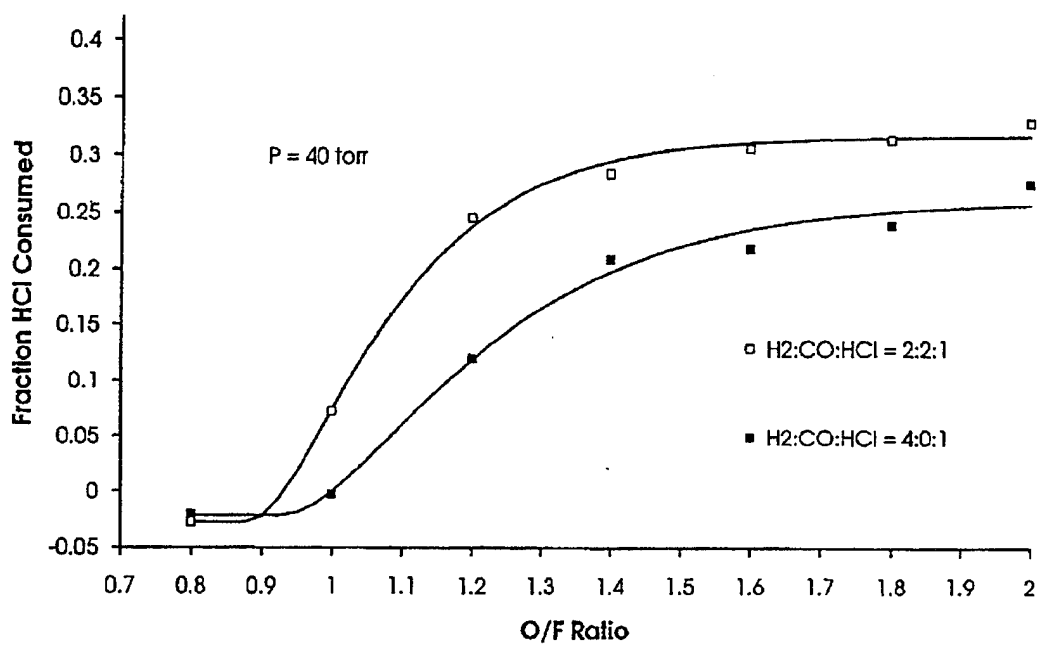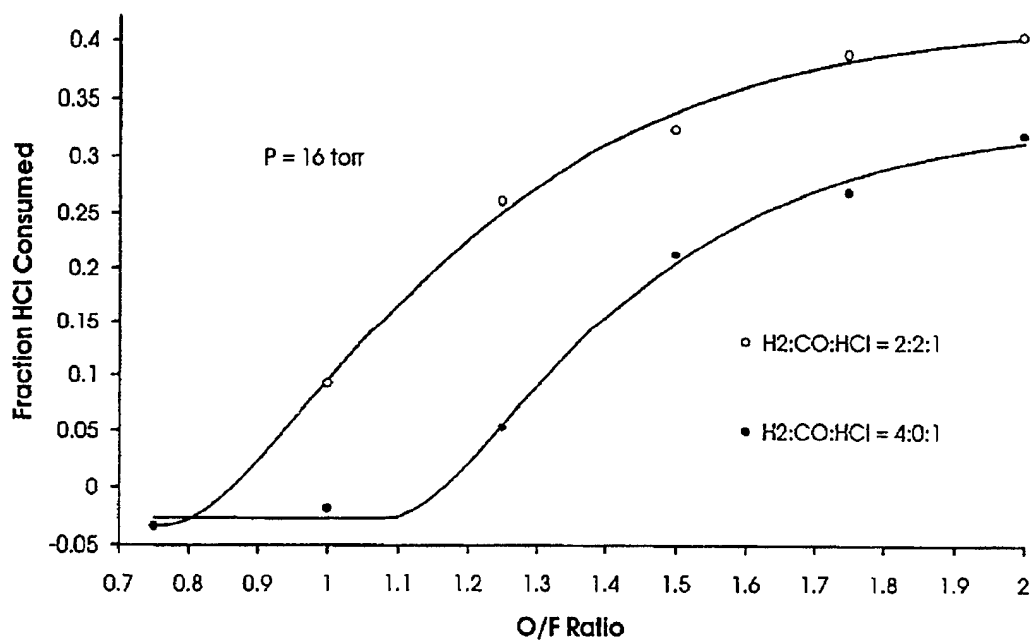| Pressure (torr)/ Altitude (km)	HCl Fractional Conversion	
	Laboratory Flame at O/F=2.0	Plume Model [1]
40 / 20		
H_2:CO:HCl = 4:0:1	0.28	
H_2:CO:HCl = 2:2:1	0.33	0.38
16 / 26		
H_2:CO:HCl = 4:0:1	0.32	
H_2:CO:HCl = 2:2:1	0.40	0.58

Figure 3. HCl Conversion in Flames at 16 torr. The fraction of HCl consumed is shown as a function of the O/F ratio for an H_2-O_2 flame with an H_2:HCl ratio of 4:1 (filled circles), and for an H_2-CO-O_2 flame with an H_2:CO:HCl ratio of 2:2:1 (open circles).

shown in Figure 4 for a 16 torr H_2-CO-O_2 flame reflect a statistical distribution of the naturally occurring Cl^{35} and Cl^{37} isotopes expected for a Cl_2 product. The expected 70:72 ratio is 1.0:0.65, which is consistent with the measured ratio of 1.0:0.60 found via an average over all experiments where the Cl_2 product was identified.

Approximately 70% (69±8.5%) of the chlorine content of the HCl consumed in the flame was converted to Cl_2, based on calibrated mass spectrometer results. This Cl_2 yield of 70% of the HCl loss is the average over the range of flame pressures and fuel compositions examined, with no clear trend with either pressure or H_2:CO ratio. However, this yield should be considered a lower limit since the detection of Cl_2 was somewhat difficult. Initial experiments showed no evidence of Cl_2 production, and even in sets of experiments where Cl_2 formation was observed, a considerable initiation period was required before Cl_2 was detected in the mass spectrometer with reproducibly high yields. The difficulty in detecting Cl_2 may have resulted from scavenging of Cl atoms and Cl_2 by the hot metal walls of the flame apparatus, with passivation eventually resulting from the extensive corrosion that occurred during these experiments.

3.2. Emission Spectroscopy

In order to probe the chemical processes occurring in the flame region, optical emission spectra were recorded for H_2-O_2 flames, both with and without added HCl. These experiments were largely motivated by the observation that the addition of even small amounts of HCl to the H_2-O_2 flame led to dramatic color and intensity changes. Without HCl, the flame was a dim blue near the burner and a dim red a few inches downstream. With HCl, the flame gave a bright white emission extending from the burner to beyond the viewable region, at least a foot downstream. The intensity of this visible emission was generally insensitive to the O/F ratio of the flame.

Spectra covering the region from 250 to 900 nm were recorded for slightly oxygen-rich H_2-O_2 flames, both without and with HCl added to the flame. Figures 5 and 6 display these spectra, which have been corrected for the calibrated variation of instrumental sensitivity with wavelength. The OH $A{\rightarrow}X$ emission at 310 nm and the Δv=4 emissions from highly vibrationally excited H_2O at wavelengths longer than 700 nm are the most intense features. These emissions are not significantly affected by the introduction of HCl into the flame, but the addition of HCl induces a broad emission continuum at wavelengths longer than 300 nm, which increases essentially linearly with wavelength out to the longest wavelength examined of 900 nm. This continuum is the apparent cause of the bright white glow observed from the HCl-seeded flame.

The HCl-induced flame emission does have some banded structure to it, with particularly distinct bands in the region near 600 nm. A series of bands from 590 to 630 nm (Figure 7) are very similar to the emissions observed by Clyne and Stedman and by Browne and Ogryzlo for Cl atom recombination in the afterglow of discharge flow systems [16,17]. This series of emission bands has been previously assigned to $B{\rightarrow}X$ emission of Cl_2, and some of the contributing, overlapping transitions in this region are shown in Figure 7 [16]. This Cl_2 emission is consistent with our mass spectrometric finding that Cl_2 is a major product of HCl-seeded flames.

Additional weak emission bands of the ClO $A{\rightarrow}X$ transition have been identified in the 355–415 nm region (Figure 8). The band positions noted match very well those assigned by Pannetier and Gaydon to ClO emissions from a Cl_2-seeded H_2-O_2 flame [18,19]. In our spectra, the ClO bands are on the rising edge of the continuum emission, which makes them somewhat indistinct. The ClO emission bands observed by Pannetier and Gaydon were also superposed on a "fairly strong continuous background" [18].

11
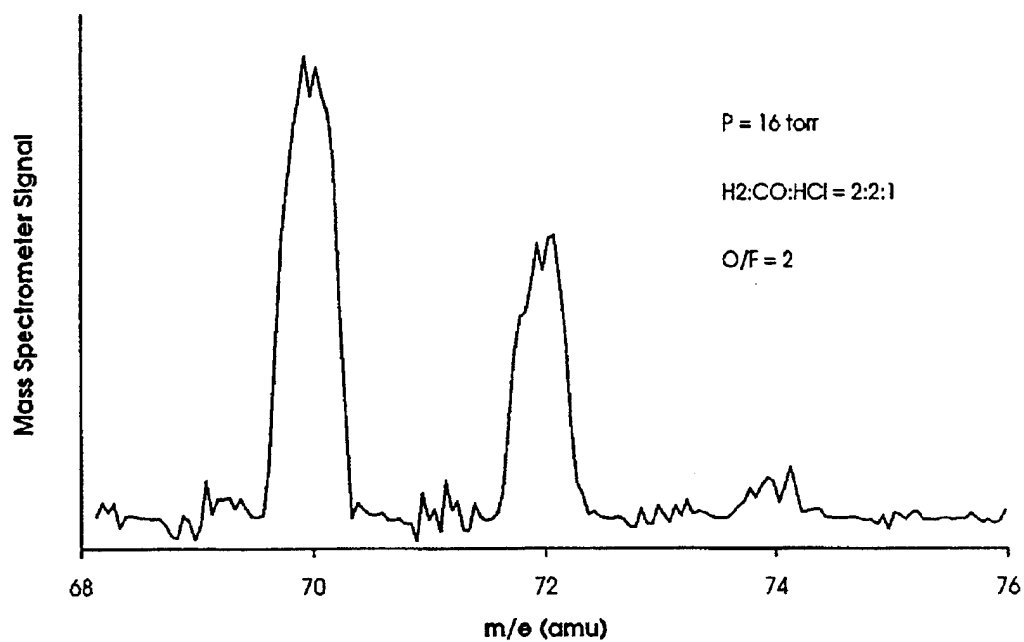
Figure 4.   Cl$_2$ Product Signal for HCl-Seeded H$_2$-CO-O$_2$ Flame. The mass
spectrometer signal from 68 to 76 a.m.u. is indicative of Cl$_2$ production
in this 16 torr flame with an H$_2$:CO:HCl ratio of 2:2:1 and O/F of 2.

12
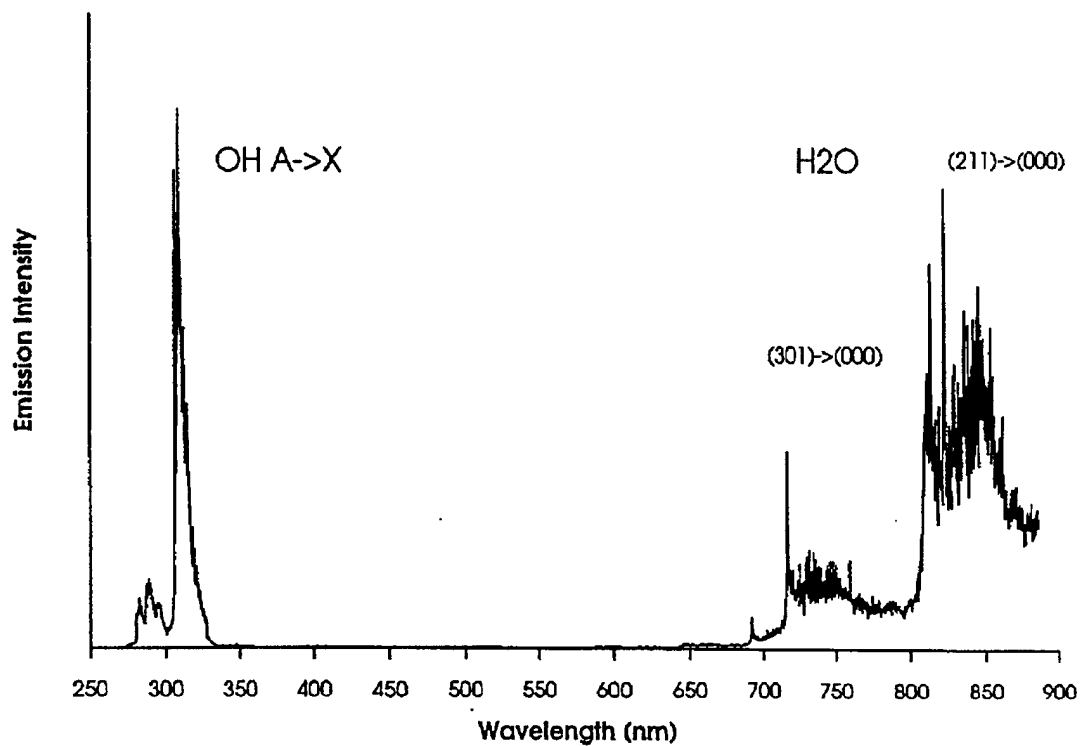
Figure 5.   Optical Emission from H_2-O_2 Flame. Emission spectra from 275 to 900 nm are shown for a 30 torr H_2-O_2 flame with O/F=1.3. Spectra have been corrected for the wavelength-dependent spectrometer sensitivity.
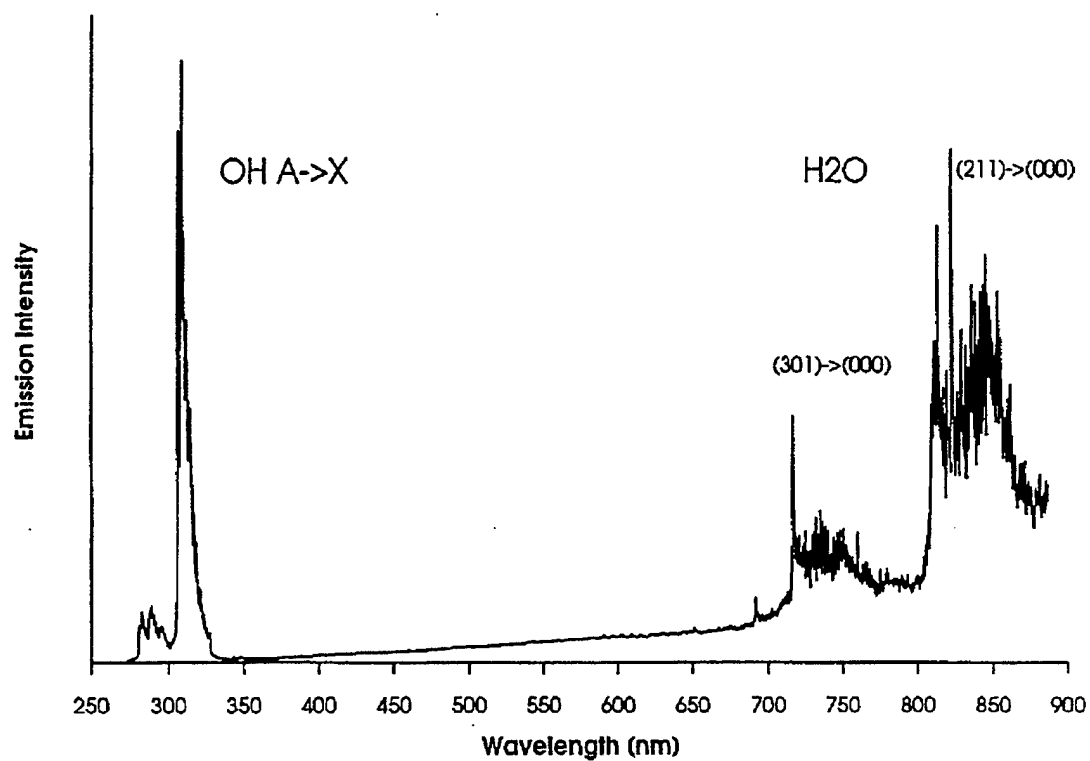
Figure 6.   Optical Emission from HCl-Seeded H_2-O_2 Flame. Emission spectra
from 275 to 900 nm are shown for a 30 torr HCl-seeded H_2-O_2 flame
with an H_2:HCl ratio of 4.5:1 and O/F=1.3. Spectra have been
corrected for the wavelength-dependent spectrometer sensitivity.

Figure 7.   Cl$_2$ $B \rightarrow X$ Emission from HCl-Seeded H$_2$-O$_2$ Flame. Emission spectra from 580 to 640 nm are shown for a 30 torr flame. Assignments of contributing Cl$_2$ $B \rightarrow X$ bands are also shown.

15

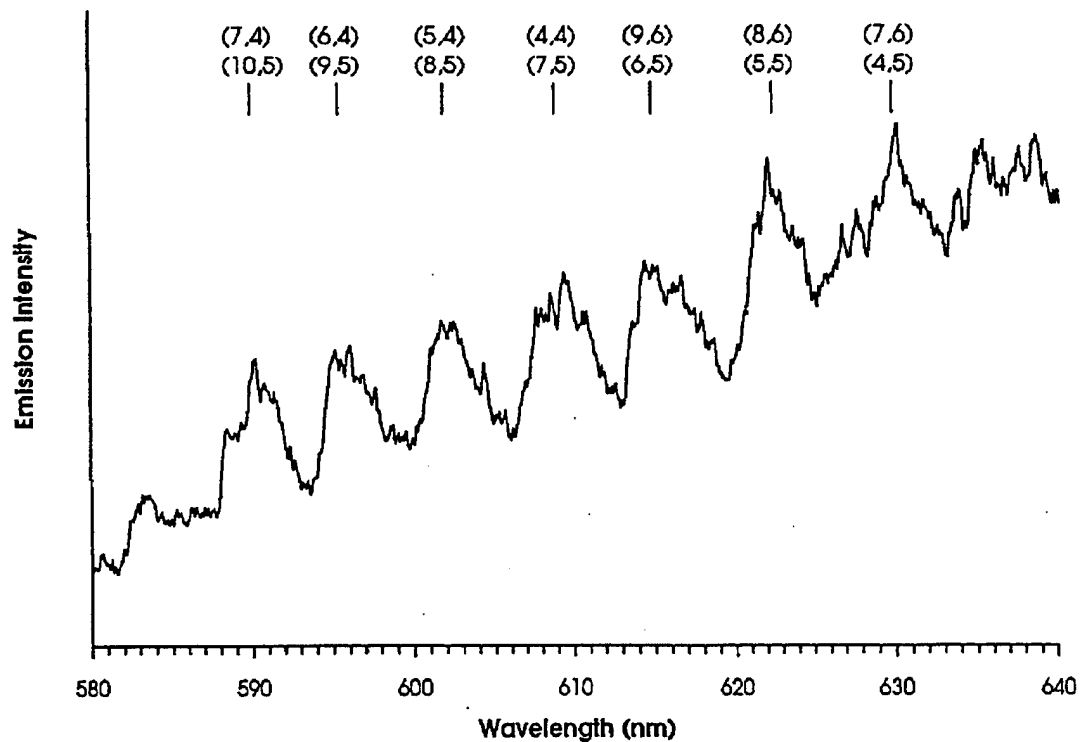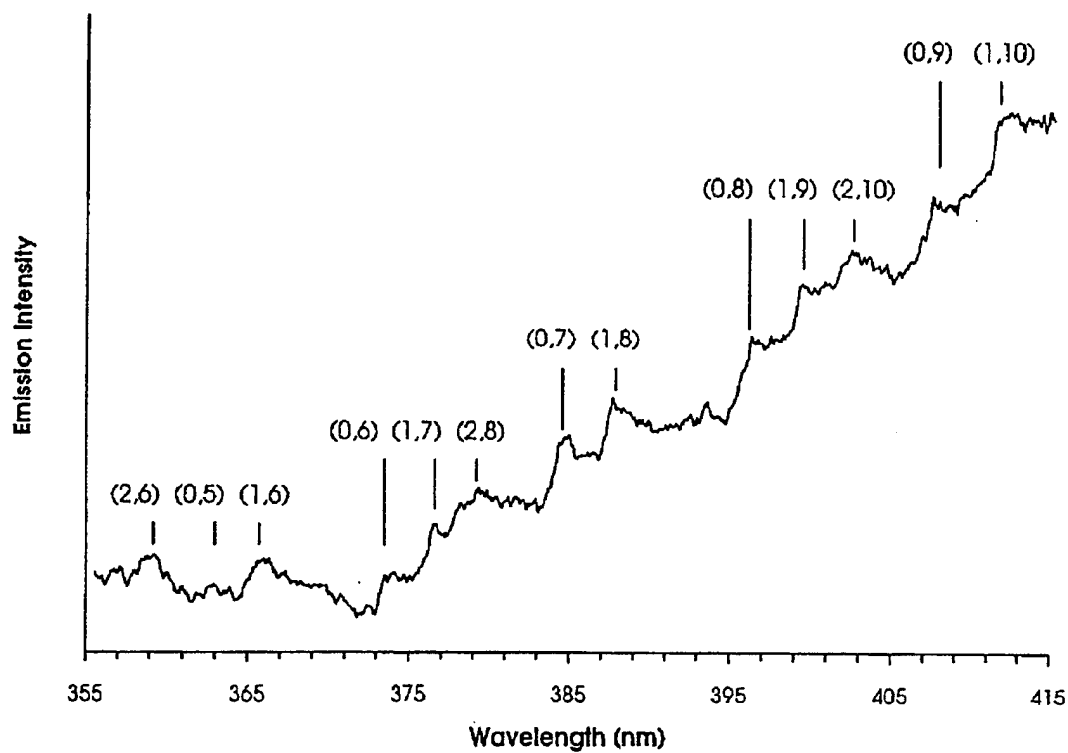Figure 8.   ClO $A \to X$ Emission from HCl-Seeded H_2-O_2 Flame. Emission spectra
from 355 to 415 nm are shown for a 30 torr flame. Tentative
assignments of ClO $A \to X$ bands are also shown.

16

The bands observed here have been reproduced on different days and were not observed in the absence of HCl, thus reinforcing their assignment as ClO emission. The band assignments noted in Figure 8 are essentially those given by Pearse and Gaydon [19], except that the v'' values have been increased by one unit in our assignment in order to improve agreement between the observed band positions and the positions calculated using the molecular constants given by Huber and Herzberg [20]. However, these assignments should be taken as tentative since the contributions of the $^2\Pi_{1/2}$ and $^2\Pi_{3/2}$ components have not been deconvolved. The observation of ClO $A \rightarrow X$ emission is not surprising, based on the highly energetic radicals and molecules in the flame and the extent of Cl_2 formation observed. ClO formation has also been predicted in model studies of stratospheric SRM afterburning, with concentrations at the level of a few percent of that predicted for Cl_2 [1].

The source of the broad continuum emission is rather uncertain. It may be due in part to unresolved Cl_2 $B \rightarrow X$ emission bands. However, the blue limit of the banded $B \rightarrow X$ emission is 478 nm, whereas the observed continuum persists to at least 350 nm. In a previous high temperature study of Cl atom recombination, a broad emission continuum was observed to persist down to 300 nm for temperatures up to 2800 K created in a shock tube [21]. This continuum emission was observed in addition to $B \rightarrow X$ emission and was assigned to the $C \rightarrow X$ transition of Cl_2 [21,22]. Only at high temperatures could a Cl_2 C state collision complex have enough energy to explain emission down to approximately 350 nm, explaining the absence of this emission at lower temperatures [16,17,21]. However, other possible origins for the continuum emission observed in these experiments cannot be ruled out, such as emissions from Cl_xO_y species. The possibility that the continuum is due to the formation of electronically excited NO_2 is unlikely, since no continuum emission is observed when there is no HCl introduced into the flame, even when air is deliberately leaked into the fuel line.

17

4. Discussion

4.1. Chemical Processes and Yields

The loss of HCl and detection of Cl_2 in the laboratory flame simulations of SRM stratospheric afterburning performed here provide at least a qualitative confirmation of model predictions by Zittel for a Titan IV SRM [1] and by Dension et al. for a smaller solid-fuel motor [3]. The most relevant experimental results to compare to the Titan IV SRM model are those for the 2:2:1 H_2-CO-HCl fuel mixture, since this composition is very similar to the 2.3:1.8:1 nozzle exhaust gas ratio used in the afterburning calculations. For pressures of 40 and 16 torr, the fractional losses of HCl observed in the laboratory were 0.33 and 0.40, respectively (Section 3.1, Table 1). The altitudes to which these pressures correspond are 20 and 26 km, respectively. Interpolating the Titan IV SRM model results to find the predicted HCl fractional losses at these altitudes yields 0.38 and 0.58, respectively. Also, for the pressure regime experimentally examined here, the models of both Zittel [1] and Denison et al. [3] predict that the chlorine liberated via HCl consumption ends up almost exclusively in the form of Cl_2. In these laboratory experiments, Cl_2 is the only chlorine-containing product detected via mass spectrometry, and its abundance accounts for at least 70% of the HCl consumed.

Experimental results thus agree qualitatively with model results concerning the magnitude of conversion of HCl under stratospheric afterburning conditions, and also concerning the production of Cl_2. The trend of increasing HCl conversion with decreasing pressure, or increasing altitude, is also in agreement. Thus, although the pressure regime examined in the laboratory corresponds to the lower-to-middle stratosphere only, the experimental results give no reason to doubt the model prediction that the extent of conversion of HCl continues to increase up to at least an altitude of 40 km [1]. Quantitatively, however, the model predicts a higher loss of HCl than observed in the laboratory, particularly at low pressure (Table 1). Part of the source of this discrepancy may be that the O/F ratios examined in the laboratory may not have extended to high enough values. Upon examination of Figure 3, it may be inferred that considerably higher losses of HCl may have been achieved if O/F ratios greater than 2 had been examined.

Another possible source of differences between model and experimental results is that the laboratory experiments did not fully reproduce the thermal and concentration gradient structure of the afterburning plume that was considered in the model. In the laboratory flame system, the fuel and oxygen were premixed, and only mixed with N_2 downstream of the burner. For afterburning plumes, however, the combustible exhaust gases mix with O_2 and N_2 in the surrounding atmosphere, creating a range of effective O/F values and introducing more of the essentially inert N_2 into the combustion region. Also, the viscous effects of turbulent mixing were not reproduced in the laboratory, with the resulting heating of plume gases being a possible source of differences. Finally, the overall composition is somewhat different for the laboratory and model systems in that, for safety reasons, the lowest N_2:O_2 ratio used experimentally was 7.5:1 (at O/F=2). This is considerably higher than the atmospheric ratio of 3.7:1, and would mainly affect the flame temperature achieved. Considering these differences, the agreement between the experimental and model results should be considered to be quite good.

These experimental results suggest that the simple description of chlorine chemistry used in the plume afterburning models [1,3] provides a fair representation of the distribution of major chlorine species left in an SRM wake at stratospheric altitudes. The models generate free chlorine primarily through the attack on HCl by OH, O, and H, all of which are produced in abundance by the combustion of H_2. These reactions are fast [23] and either exothermic or nearly thermoneutral at the temperatures above 2000 K

19

typically modeled for an afterburning SRM plume at an altitude of 20 km. The predicted concentrations of minor chlorine-containing species, e.g., ClO and ClO_2, may be less certain, requiring more complex reaction paths. However, the impact on ozone loss of the direct production of these species through afterburning is minor. The application of the plume afterburning models to a direct simulation of the laboratory flame may be possible and is under study.

The radiative emission observed from HCl-seeded flames provides insight into the chemical reactivity of HCl. Both continuum and banded emission were observed to be induced by the addition of HCl, with all of this emission apparently arising from chlorine-containing compounds. The character of this emission did not vary dramatically with O/F, even if the fraction of HCl consumed changed from 0.0 to 0.4. Thus, it appears that the HCl in the flame is undergoing dynamic conversion to and from other chlorine-containing compounds at all O/F values examined. This is a consequence of the high temperatures of over 2000 K achieved in the flame, in that both forward and reverse reaction rates are high, and thus a local equilibrium is closely approached in the hottest regions of the flame. This view is supported by the finding of Roesler, Yetter, and Dryer that the primary reactions liberating Cl from HCl rapidly reached equilibrium in their reaction system [12,13], which at 1000 K was significantly cooler than the flame used here. Assuming local equilibrium in the hottest flame regions, the final HCl conversion should be controlled by both the kinetics and thermodynamics of the downstream cooling region.

4.2. Implications for Environmental Impact

Insofar as our experimental results support model predictions that large amounts of Cl and Cl_2 may be formed via SRM afterburning, the findings of this laboratory study indicate that local ozone concentrations may be significantly lowered near the path of the launch vehicle. Modeling studies of the plume expansion and chemistry in the minutes to hours following the passage of an SRM should thus use a Cl_2-rich starting composition, as predicted by plume afterburning codes.

The detailed impact of the deposition of this "free" chlorine on stratospheric ozone is a matter to be evaluated through modeling and/or field experimentation. The latter is preferred in that it would provide information as to the extent of conversion of HCl to Cl_2 via afterburning in a real plume, and also would determine the local impacts to ozone concentrations. A variety of experimental approaches has been proposed at this point, including ground-based UV absorption measurements, lidar, and several in-situ methods. The proposed in-situ methods include mass spectrometric sampling, UV absorption, IR absorption, and NO chemiluminescence. The launch of a large vehicle such as a Titan IV or a Space Shuttle would be ideal to investigate, since these vehicles have greater potential for ozone impact as compared to smaller launch vehicles.

The flame optical emissions observed in this present study could, in theory, be used as a probe of the afterburning chemistry of exhaust plumes, but in practice, may be difficult to employ. These emissions will certainly be overwhelmed throughout much of the visible part of the spectrum by the thermal radiation from micron-sized alumina particles. These particles are produced in abundance by the SRM. Also, for a daytime launch, solar scattering will interfere at the wavelengths short of 400 nm, where alumina thermal emissions will be least severe. Furthermore, the constant intensity of the HCl-induced flame emission over a broad range of conversion indicates that even if this emission were observed for an afterburning plume, it would not allow the net loss of HCl to be quantified.

20

5. Summary and Conclusions

A laboratory flame apparatus was used to simulate stratospheric afterburning of a SRM plume. It was found that under oxygen-rich conditions, a large fraction of the HCl injected into the flame was converted to Cl_2, whereas under fuel-rich conditions, no HCl was lost. Both the loss of HCl and the formation of Cl_2 were quantified via mass spectrometry, with HCl losses up to 40% observed. At least 70% of the chlorine liberated from the loss of HCl was converted to Cl_2. Emission spectra recorded from 275 to 900 nm contain distinct Cl_2 $B{\rightarrow}X$ bands, along with minor ClO $A{\rightarrow}X$ bands and a broad continuum induced by the presence of chlorine-containing compounds in the flame. The insensitivity of the emission intensities to the oxygen content of the flame indicates that HCl and other chlorine-containing compounds were undergoing a dynamic interconversion in the flame, even under conditions where there was little or no net loss of HCl.

For flame fuel compositions that closely simulated the gaseous components of the exhaust from SRMs, the magnitude of the loss of HCl observed in the laboratory is similar to that predicted by plume afterburning models. The trend predicted by models, where the extent of HCl conversion increases with altitude, was also confirmed in the laboratory via experiments at different flame pressures. Quantitative differences between experimental and model results may be due primarily to differences in structure and composition between the laboratory flame and the model plume.

Considering the agreement between afterburning model predictions and the results of this laboratory study, the use of these model predictions as initial conditions for calculations of the environmental impact of launches appears to be justified. To further assess launch environmental impact, field experiments will be required. These experiments would allow the extent of HCl conversion in real plumes to be determined, along with the resulting effect on the local ozone concentrations.

References

[1] Zittel, P. F. *Computer Model Predictions of the Local Effects of Large, Solid-Fuel Rocket Motors on Stratospheric Ozone*, Aerospace Technical Report TR-94(4231)-9, The Aerospace Corporation, September 1994.

[2] Martin, L. R. *Possible Effect of the Chorine Oxide Dimer on Transient Ozone Loss in Rocket Plumes*, Aerospace Technical Report TR-94(4231)-1, March 1994.

[3] Denison, M. R., Lamb, J. J., Bjorndahl, W. D., Wong, E. Y., and Lohn, P. D. *J. Spacecraft and Rockets* 31:435 (1994).

[4] Ross, M. N. *J. Spacecraft and Rockets* in press.

[5] Karol, I. L., Ozolin, Y. E., and Rozanov, E. V. *Ann. Geophysicae* 10:810 (1992).

[6] Kruger, B. C. *Ann. Geophysicae* 12:409 (1994).

[7] Danilin, M. Y. *Ann. Geophysicae* 11:828 (1993).

[8] Jones, A. E., Bekki, S., and Pyle, J. A. *J. Geophys. Res.,* in press.

[9] Blackmore, D. R., O'Donnell, G., and Simmons, R. F. *Tenth Symposium (International) on Combustion*, The Combustion Institute, Pittsburgh, 1964, p. 303.

[10] Butlin, R. N., and Simmons, R. F. *Combust. Flame* 12:447 (1968).

[11] Dixon-Lewis, G., and Simpson, R. J. *Sixteenth Symposium (International) on Combustion*, The Combustion Institute, Pittsburgh, 1976, p. 1111.

[12] Roesler, J. F., Yetter, R. A., and Dryer, F. L. *Combust. Sci. and Tech.* 82:87 (1992).

[13] Roesler, J. F., Yetter, R. A., and Dryer, F. L. *Combust. Sci. and Tech.* 85:1(1992).

[14] Roesler, J. F., Yetter, R. A., and Dryer, F. L. *Combust. Flame* 100:95 (1995).

[15] Pritt, A. T., Osibov, M. N., Poole, R. B., and Presser, N. *Proc. 20th JANNAF Exhaust Plume Technology Subcommittee Meeting* 1:533 (1993).

[16] Clyne, M. A. A., and Stedman, D. H. *Trans. Faraday Soc.* 64:1816 (1968).

[17] Browne, R. J., and Ogryzlo, E. A. *J. Chem. Phys.* 52:5774 (1970).

[18] Pannetier, G., and Gaydon, A. G. *Nature* 161:242 (1948).

[19] Pearse, R. W. B., and Gaydon, A. G. *The Identification of Molecular Spectra.* 4th ed., Chapman and Hall, London, 1976.

[20] Huber, K. P., and Herzberg, G. *Molecular Spectra and Molecular Structure, IV. Constants of Diatomic Molecules.* Van Nostrand Reinhold, New York, 1979.

[21] Belokrinitskij, N. S., Kernazitskij, L. A., and Shpak, M. T. *Chem. Phys. Lett.,* 72, 199 (1980).

[22] In reference [21], short wavelength continuum emission is attributed to the $^1\Pi_u$ state of Cl_2; although this state is designated as A in reference [21], it is more customary to designate it as C [20].

[23] Mallard, W. G., Westley, F., Herron, J. T., Hampson, R. F., and Frizzell, D. H., *NIST Chemical Kinetics Database: Version 6.0*, NIST, Gaithersburg, MD, 1994.

TECHNOLOGY OPERATIONS

The Aerospace Corporation functions as an "architect-engineer" for national security programs, specializing in advanced military space systems. The Corporation's Technology Operations supports the effective and timely development and operation of national security systems through scientific research and the application of advanced technology. Vital to the success of the Corporation is the technical staff's wide-ranging expertise and its ability to stay abreast of new technological developments and program support issues associated with rapidly evolving space systems. Contributing capabilities are provided by these individual Technology Centers:

Electronics Technology Center: Microelectronics, VLSI reliability, failure analysis, solid-state device physics, compound semiconductors, radiation effects, infrared and CCD detector devices, Micro-Electro-Mechanical Systems (MEMS), and data storage and display technologies; lasers and electro-optics, solid state laser design, micro-optics, optical communications, and fiber optic sensors; atomic frequency standards, applied laser spectroscopy, laser chemistry, atmospheric propagation and beam control, LIDAR/LADAR remote sensing; solar cell and array testing and evaluation, battery electrochemistry, battery testing and evaluation.

Mechanics and Materials Technology Center: Evaluation and characterization of new materials: metals, alloys, ceramics, polymers and composites; development and analysis of advanced materials processing and deposition techniques; nondestructive evaluation, component failure analysis and reliability; fracture mechanics and stress corrosion; analysis and evaluation of materials at cryogenic and elevated temperatures; launch vehicle fluid mechanics, heat transfer and flight dynamics; aerothermodynamics; chemical and electric propulsion; environmental chemistry; combustion processes; spacecraft structural mechanics, space environment effects on materials, hardening and vulnerability assessment; contamination, thermal and structural control; lubrication and surface phenomena; microengineering technology and microinstrument development.

Space and Environment Technology Center: Magnetospheric, auroral and cosmic ray physics, wave-particle interactions, magnetospheric plasma waves; atmospheric and ionospheric physics, density and composition of the upper atmosphere, remote sensing using atmospheric radiation; solar physics, infrared astronomy, infrared signature analysis; effects of solar activity, magnetic storms and nuclear explosions on the earth's atmosphere, ionosphere and magnetosphere; effects of electromagnetic and particulate radiations on space systems; space instrumentation; propellant chemistry, chemical dynamics, environmental chemistry, trace detection; atmospheric chemical reactions, atmospheric optics, light scattering, state-specific chemical reactions and radiative signatures of missile plumes, and sensor out-of-field-of-view rejection.